Low-Reynolds Number Effects in Backward-Facing Step Flow using Large Eddy Simulations

Davidson, L.; Nielsen, Peter Vilhelm

Publication date:
1998

Document Version
Publisher's PDF, also known as Version of record

Aalborg **UNIVERSITY**

Low-Rey

Low-Reynolds Number Effects in Backward-Facing Step Flow Using Large Eddy Simulations

Lars Davidson, Peter V. Nielsen

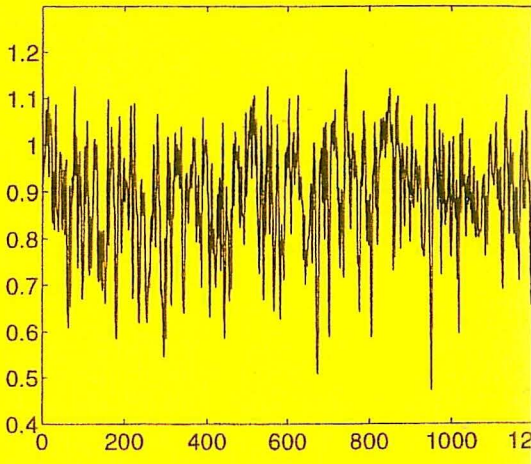

Indoor Environmental Engineering, Oktober 1998
Department of Building Technology and Structural Engineering
ISSN 1395-7953 R9842

Low-Reynolds Number Effects in Backward-Facing Step Flow Using Large Eddy Simulations

Lars Davidson, Peter V. Nielsen

Printed at Aalborg University

Low-Reynolds Number Effects in Backward-Facing Step Flow Using Large Eddy Simulations

Lars Davidson*
Dept. of Thermo and Fluid Dynamics
Chalmers University of Technology
S-412 96 Gothenburg, Sweden
http://www.tfd.chalmers.se/~lada

Peter V. Nielsen
Dept. of Building Technology and Structural Engineering
Aalborg University
Sohngaardsholmsvej 57
DK-9000 Aalborg, Denmark
http://www.civil.auc.dk/i6/staff/navn/i6pvn.html

October 12, 1998

1 Abstract

The flow in ventilated rooms is often not fully turbulent, but in some regions the flow can be laminar. Problems have been encountered when simulating this type of flow using RANS (Reynolds Averaged Navier-Stokes) methods. Restivo [1] carried out experiment on the flow after a backward-facing step, with a large step (the ratio of the total height to the inlet is 6). This is much larger than what is common for backward-facing flow. The reason why Restivo chose this configuration is that it is similar to a ventilated room with the opposite wall removed. Detailed measurements were carried out in Ref. [1] at $Re = 117, 780$ and $Re = 5000$. For the lowest Reynolds number the flow was fully laminar. At the intermediate Reynolds number the flow was partially, although not fully, turbulent. At the highest Reynolds number the flow was found to be fully turbulent. Thus we can identify three types of flows: laminar, transitional, and fully turbulent.

*This work was carried out during the author's stay at Dept. of Building Technology and Structural Engineering, Aalborg University in Autumn 1997.

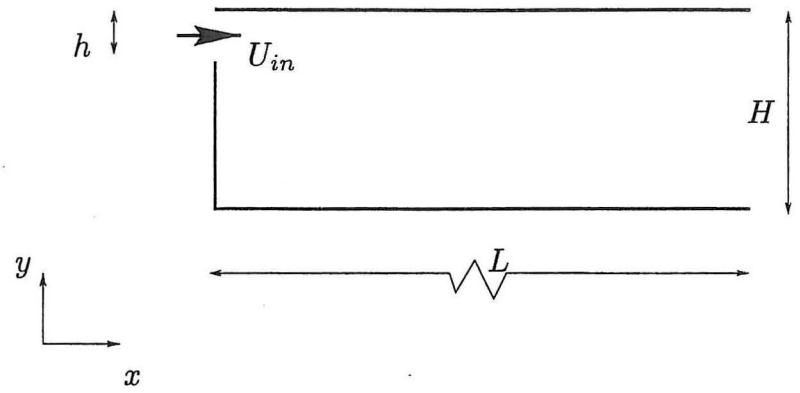

Figure 1: Configuration. Extent in z direction is $0 \leq z \leq W$.

2 Introduction

In the present study this flow will be computed using Large Eddy Simulations (LES). We have chosen the two Reynolds numbers investigated in Ref. [1] ($Re =$ 780 and 5000). Previously we have computed fully turbulent flow in a ventilated room using LES with good results [2]. A considerably more efficient numerical solver is used in the present study [3]. A dynamic one-equation model is used as a subgrid model [4].

Initially, we planned to also present simulations of the lowest Reynolds number $Re = 117$ (i.e. laminar flow). However, it turned out that when the numerical predictions of the laminar flow were compared to the experiments of Restivo [1], we found a large discrepancy. This work is presented in Ref. [5]. We believe that there is something wrong in that experimental investigation. To support that conclusion, we present in Ref. [5] predictions of other backward facing flow configurations, where we show that our predictions agree well with experimental data.

In the following sections we present the subgrid model, the numerical method and results and discussions.

3 The Dynamic One-Equation Subgrid Model

Recently a new dynamic one-equation subgrid model was presented [4]. For convenience, the model is briefly described below.

The modelled k_{sgs} equation can be written

$$\frac{\partial k_{sgs}}{\partial t} + \frac{\partial}{\partial x_j}(\bar{u}_j k_{sgs}) = \frac{\partial}{\partial x_j}\left(\langle C\rangle_{xyz}\Delta k_{sgs}^{\frac{1}{2}}\frac{\partial k_{sgs}}{\partial x_j}\right) + 2\nu_{sgs}\bar{S}_{ij}\bar{S}_{ij} - C_*\frac{k_{sgs}^{\frac{3}{2}}}{\Delta} \tag{1}$$

In the production term, the dynamic coefficient C

$$P_{k_{sgs}} = -\tau_{ij}^a \bar{u}_{i,j}, \quad \bar{S}_{ij} = \frac{1}{2}\left(\frac{\partial \bar{u}_i}{\partial x_j} + \frac{\partial \bar{u}_j}{\partial x_i}\right)$$
$$\tau_{ij}^a = -2C\Delta k_{sgs}^{\frac{1}{2}}\bar{S}_{ij} = -2\nu_{sgs}\bar{S}_{ij} \tag{2}$$

is computed in a way similar to that used in the standard dynamic model [6, 7, 8, 9], i.e.

$$
\begin{aligned}
C &= -\frac{\mathcal{L}_{ij}M_{ij}}{2M_{ij}M_{ij}}, \quad \mathcal{L}_{ij} = \widehat{\bar{u}_i\bar{u}_j} - \widehat{\bar{u}}_i\widehat{\bar{u}}_j \\
K &= \widehat{k}_{sgs} + \frac{1}{2}\mathcal{L}_{ii}, \quad M_{ij} = \widehat{\Delta}\widehat{K^{\frac{1}{2}}}\widehat{\bar{S}}_{ij} - \Delta\widehat{k_{sgs}^{\frac{1}{2}}\bar{S}_{ij}}
\end{aligned}
\tag{3}
$$

where $\mathcal{L}_{ij}$ denotes the *dynamic* Leonard stresses, and where $K \equiv \frac{1}{2}T_{ii}$ is the subgrid kinetic energy on the test level [8, 9, 10].

To ensure numerical stability, a *constant* value of C in space ($\langle C\rangle_{xyz}$) is used in the momentum equations. This is determined by requiring that the production in the whole computational domain should remain the same, i.e.

$$
\langle 2C\Delta k_{sgs}^{\frac{1}{2}}\bar{S}_{ij}\bar{S}_{ij}\rangle_{xyz} = 2\langle C\rangle_{xyz}\langle\Delta k_{sgs}^{\frac{1}{2}}\bar{S}_{ij}\bar{S}_{ij}\rangle_{xyz} \tag{4}
$$

The idea is to include all local dynamic information through the source terms of the transport equation for k_{sgs}. This is probably physically more sound since large local variations in C appear only in the source term, and the effect of the large fluctuations in the dynamic coefficients will be smoothed out in a natural way. In this way, it turns out that the need to restrict or limit the dynamic coefficient is eliminated altogether.

4 The Numerical Method

An implicit, two-step time-advancement methods is used [3]. The filtered Navier-Stokes equation for the $\bar{u}_i$ velocity reads

$$
\frac{\partial\bar{u}_i}{\partial t} + \frac{\partial}{\partial x_j}\left(\bar{u}_i\bar{u}_j\right) = -\frac{1}{\rho}\frac{\partial\bar{p}}{\partial x_i} + \nu\frac{\partial^2\bar{u}_i}{\partial x_j\partial x_j} - \frac{\partial\tau_{ij}}{\partial x_j} \tag{5}
$$

When it is discretized it can be written

$$
\begin{aligned}
\bar{u}_i^{n+1} = \bar{u}_i^n &+ \Delta t H\left(\bar{u}_i^n, \bar{u}_i^{n+1}\right) - \frac{1}{\rho}\alpha\Delta t\frac{\partial\bar{p}^{n+1}}{\partial x_i} \\
&- \frac{1}{\rho}(1-\alpha)\Delta t\frac{\partial\bar{p}^n}{\partial x_i}
\end{aligned}
\tag{6}
$$

where $H\left(\bar{u}_i^n, \bar{u}_i^{n+1}\right)$ includes convection and the viscous and subgrid stresses, and $\alpha = 0.5$ (Crank-Nicolson). Equation 6 is solved which gives $\bar{u}_i^{n+1}$ which does not satisfy continuity. An intermediate velocity field is computed by subtracting the implicit part of the pressure gradient, i.e.

$$
\bar{u}_i^* = \bar{u}_i^{n+1} + \frac{1}{\rho}\alpha\Delta t\frac{\partial\bar{p}^{n+1}}{\partial x_i}. \tag{7}
$$

Taking the divergence of Eq. 7 requiring that continuity (for the face velocities $\bar{u}_{i,f}^*$ which are obtained by linear interpolation) should be satisfied on level $n+1$, i.e. $\partial\bar{u}_{i,f}^{n+1}/\partial x_i = 0$ we obtain

$$
\frac{\partial^2\bar{p}^{n+1}}{\partial x_i\partial x_i} = \frac{\rho}{\Delta t\alpha}\frac{\partial\bar{u}_{i,f}^*}{\partial x_i}. \tag{8}
$$

Mesh	Re	$\frac{\Delta x_{min}}{H}$	$\frac{\Delta x_{max}}{H}$	$\frac{\Delta y_{min,f}}{H}$	$\frac{\Delta y_{min,c}}{H}$	$\frac{\Delta y_{max}}{H}$	$\frac{\Delta z}{H}$	L
$160 \times 80 \times 64$	$Re = 780$	0.013	0.20	0.0016	0.043	0.04	0.047	$17.5H$
$128 \times 80 \times 80$	$Re = 5000$	0.013	0.17	0.0016	0.043	0.04	0.0375	$11.5H$
$128 \times 80 \times 128$	$Re = 5000$	0.013	0.17	0.0016	0.043	0.04	0.0234	$11.5H$

Table 1: Geometrical details of the meshes. The *min* denote the extent of the near-wall cell. Index c and f denote ceiling and floor, respectively.

5 Results

The configuration is shown in Fig. 1. The geometry is given by:

$$W/H = 3,\ h/H = 1/6,\ Re = \frac{U_{in}h}{\nu}$$

Air of 20^oC is used, and $H = 3$ m. We use no-slip at all walls. $y^+ < 2$ at the west wall, the floor and the ceiling; mostly it is below one. Near the side walls (low and high z) y^+ is around 10. If $y^+ > 11$, wall functions are used [11]. The subgrid kinetic energy is set to zero at all walls as well as at the inlet. A convective boundary condition is used at the outlet for $\bar{u}$, i.e.

$$\frac{\partial \bar{u}}{\partial t} + U_b \frac{\partial \bar{u}}{\partial x} = 0.$$

where U_b it the bulk velocity ($= U_{in}h/H$). This boundary condition has shown to be considerably better than zero streamwise gradient [12]. Zero streamwise gradient is used for $\bar{v}$.

A geometric stretching is used for the grid in the y direction, with refinement near the walls. The inlet is covered by 30 cells. In the x direction the cell spacing increases with x, and in the z direction a constant spacing is used; for more details see Table 1.

For the fully turbulent case ($Re = 5000$) random fluctuation are superimposed on the experimental inlet velocity

$$\begin{aligned} \bar{u}_{in} &= U_{in} + 2\left(rnd - \frac{1}{2}\right) u'_{exp} \\ \bar{v}_{in} &= \left(rnd - \frac{1}{2}\right) u'_{exp},\ \bar{w}_{in} = \left(rnd - \frac{1}{2}\right) u'_{exp} \end{aligned} \tag{9}$$

which gives a fluctuating amplitude u'_{exp} (both positive and negative) for $\bar{u}$, and half of that for $\bar{v}$ and $\bar{w}$. The inlet velocity U_{in} is constant over the inlet.

The time step is set to 0.26 seconds and 1.8 seconds for $Re = 5000$ and $Re = 780$, respectively. This gives a maximum convective CFL number of approximately one.

For $Re = 5000$, two different grids (one coarse and one fine) have been used. The number of cells in the z direction has been increased on the fine mesh. Unless otherwise stated, the results from the coarse mesh are presented below.

The fine-mesh computations have been carried out on a 64 processesor ORIGIN 2000 at Chalmers. The code was parallelized by Zacharov [13]. Using

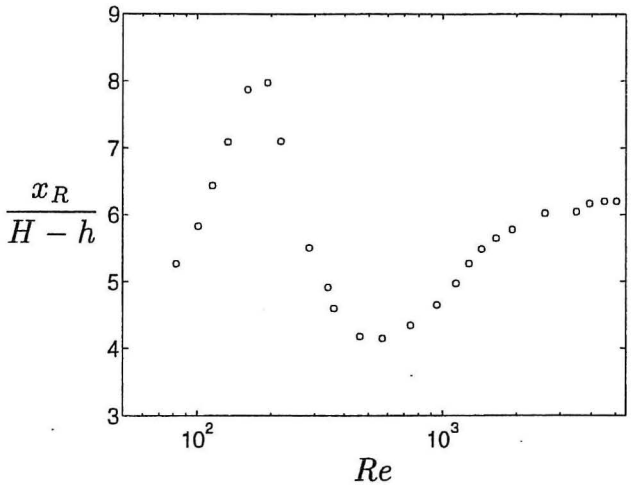

Figure 2: Experimental reattachment length x_R as a function of inlet Reynolds number Re [1].

one/four/eight processors the elapsed time was 177/52/28 seconds per time step, thus giving a speed-up of 3.5 and 6.3 on four and eight processors, respectively.

The one-equation subgrid model presented above is used. The average value of the homogeneous constant in Eq. 4 is $\langle C \rangle_{xyz} \simeq 0.07$ for $Re = 780$ and $\langle C \rangle_{xyz} \simeq 0.075$ for $Re = 5000$.

Vector plots are presented in Fig. 3. As can be seen the recirculation bubble is large for $Re = 780$ ($x_R/(H-h) = 9.2$). As a result the secondary bubble below the inlet is also large. The experimental data show the reverse: the recirculation region is larger for $Re = 5000$ than for $Re = 780$, see Fig. 2. However, also the experiments show a larger bubble if the Reynolds number is reduced even further (down to $Re \lesssim 250$). Other experimental investigations do not show such a marked dip in the $x_R - Re$ curve as shown in Fig. 2. For example, neither the experimental investigation by Armaly *et al.* [14] nor by Romano *et al.* [15] present any similar dip. It should, however, be kept in mind the the step was smaller in these two investigations ($h/H = .514$ and $2/3$, respectively). In a separate study, the present authors predict laminar flow in the Restivo-configuration [5]. It was concluded that for low Re numbers (laminar flow) there are some problems with his measurements. Thus, considering the discrepancy between the predictions and experiments at $Re = 780$, we think that the predictions are more correct than are the experiments. In Fig. 4 the large discrepancies between prediction and experiments are further illustrated.

For $Re = 5000$ the predicted reattachment length is $x_{\bar{R}}/(H-h) = 7.3$ and 7.6 for the coarse and fine mesh, respectively. This is some 20% larger than experimental data ($x_{R,exp} = 6.12(H-h) = 30.6h$). A number of factors can explain this discrepancy: too coarse a grid, inadequate subgrid model, inaccurate inlet boundary conditions, and, inaccurate measurements. In order to investigate possible numerical errors, we present below computations with different grids, different subgrid models, and different inlet boundary conditions.

Two different grids have been used. As can be seen (Fig. 5) the difference between the predictions on the two grids is small except for $x/h \geq 35$. This is probably because the three-dimensional effects are large in the reattachment region (see Fig. 11), and these are convected downstream. In Fig. 6 predictions with two different boundary conditions are shown: 1) constant inlet profile

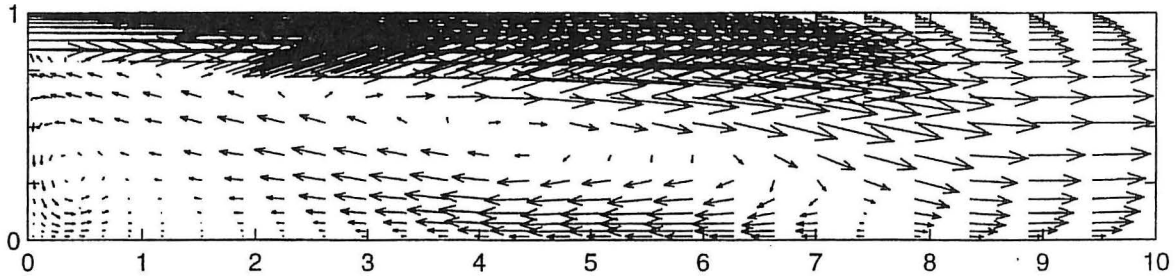

a)

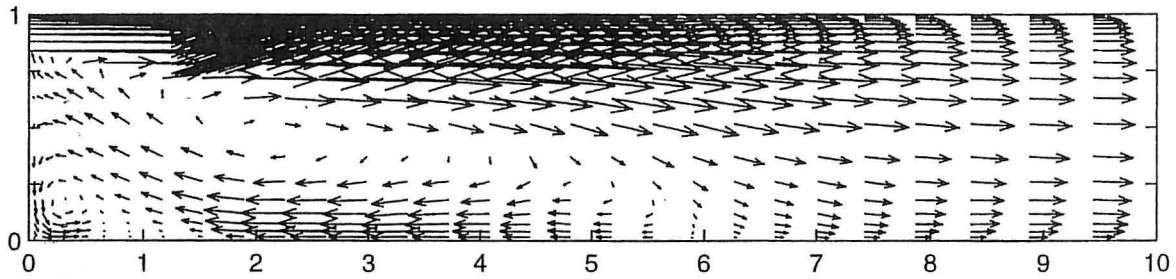

b)

Figure 3: Time-averaged velocity vector plot (not to scale). $z/W = 0.5$. Every fourth vector is plotted in each direction. a) $Re = 780$. b) $Re = 5000$.

(see Eq. 9), and 2) 1/7-profile for U_{in} in Eq. 9. In Fig. 6 the time-averaged velocity using two different subgrid models are also presented. The dynamic one-equation model is compared with the standard dynamic subgrid model Germano [6]; in the latter model the dynamic coefficient was avaraged in the spanwise direction in order to stabilize the numerical procedure, and some additional local averaging was used in the x and y direction as well. Fig. 7 present the same cases as in Fig. 6, but now the spanwise averaged ($0.5H < z < 2.5H$) $\bar{u}$ velocities are shown. The predictions presented in Figs. 5- 7 differ fairly much, but they have one thing in common: the reattachment is predicted too late compared with experiments.

It should be mentioned that the reattachment length has been accurately predicted with traditional Low-Re eddy-viscosity models such as the $k-\varepsilon$ model [16] and a modified $k-\omega$ model [17].

No problems were experienced in performing the calculations for the low Reynolds number. The inlet boundary conditions are laminar, and a transition to turbulent flow occurs somewhere further downstream. In Fig. 8, the time history of the $\bar{u}$ velocity at two points are shown which illustrates the transition. Close to the inlet ($x/H = 5/6$), the fluctuating velocities are small whereas further downstream ($x/H = 4$) they have grown much larger and the flow can be considered as turbulent. The rms-values u_{rms}/U_{in} at these two points (see Fig. 8) are 1.4% and 11.5%, respectively. The corresponding figures for $Re = 5000$ are 4.6% and 13.8%. Thus the growth of the fluctuations is much stronger for the low Re number case, in which the flow goes from laminar (the inlet), via transitional to fully turbulent. At the high Re number the flow is fully turbulent right from the inlet.

Attempts have been carried out to compute this flow at low Reynolds numbers by Skovgaard and Nielsen [16], where a low-Re number $k-\varepsilon$ was used. No convergent results were obtained for $Re < 1000$. This is probably because as k goes towards zero, the ε equation becomes ill-conditioned, because there are terms which include ε/k. Peng *et al.* [18] used $k-\omega$ models. The advantage of this type of model is that the ω equations possesses a solution even if $k \to 0$. The turbulent diffusion terms goes to zero, and the production term, the convection term, the destruction term and the viscous diffusion term balance each other. No convergence problems were reported. The same trend as in the present work was found, i.e. that the x_R increases when the Re number is reduced. In that work it was nevertheless concluded that the $k-\omega$ failed, since the agreement with experimental data was very poor for low Reynolds numbers. In view of the findings in this work (including Ref. [5]), that conclusion was perhaps incorrect.

In Fig. 5, the velocities for the coarse mesh have been time averaged during 11000 (2860 seconds) and 17000 (4420 seconds), respectively. From Fig. 5 it seems that the time during which time averaging is performed is sufficient. The number of time steps for time averaging for the fine mesh is 18000; time averaging was performed for another 6000 time steps but the effect on the time averaged $\bar{u}$ profiles was found to be negligible.

We can relate the time-averaging time to how long time T_{conv} it takes for a fluid to be convected past the recirculation region. This would correspond to a characteristic time unit. A "bulk" velocity for the flow past the recirculating region is $U_{bulk} \simeq 0.5U_{in} = 0.5 \cdot 0.153 \simeq 0.076$ m/s. Thus, we get $T_{conv} = x_R/U_{bulk} = 6 \cdot 2.5/0.076 = 197$ seconds. Thus the averaging time T_{aver} correspond to 14.5 and 22.4 characteristic time units, respectively. This should

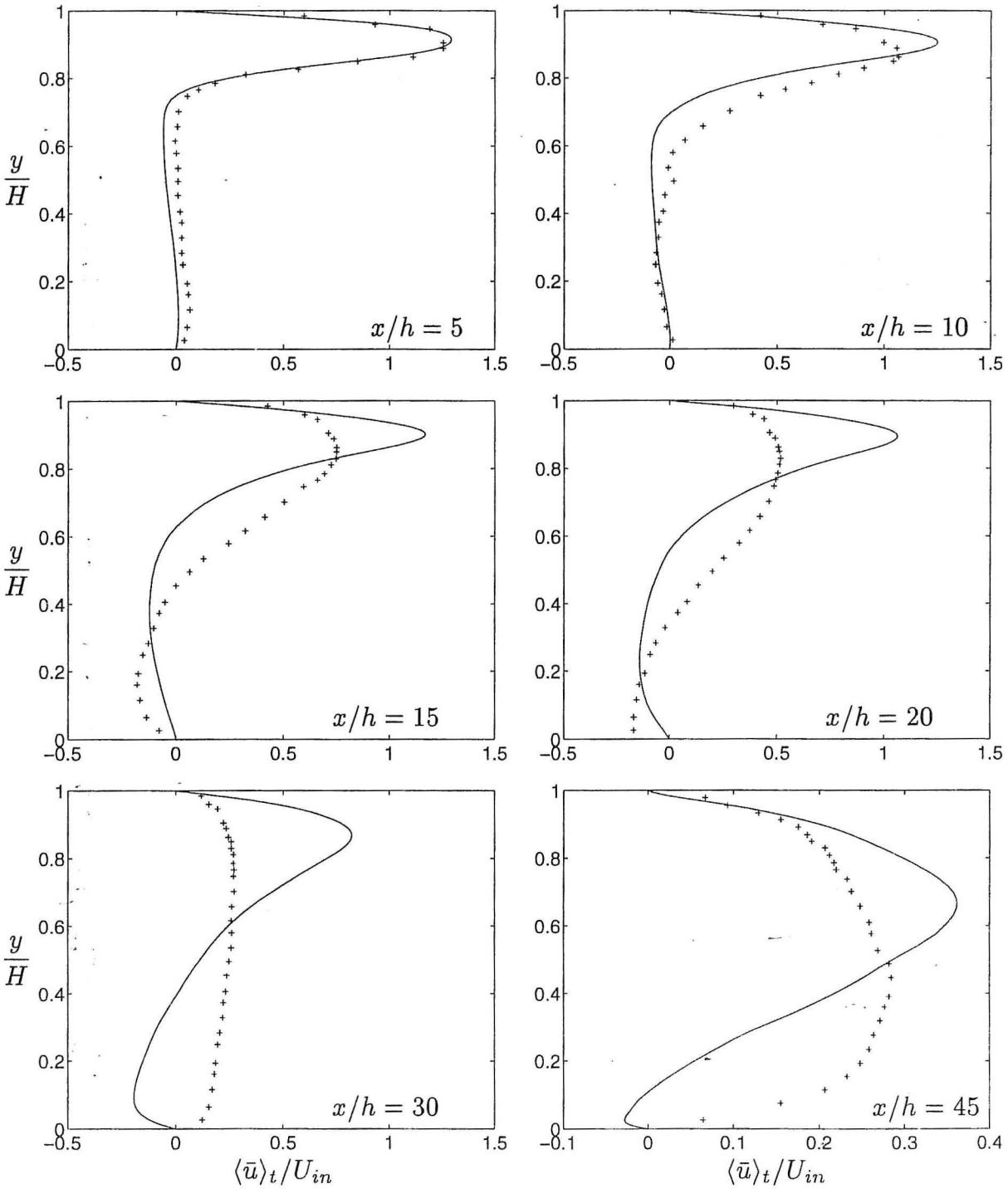

Figure 4: Time averaged streamwise velocity $\langle \bar{u} \rangle_t$. $Re = 780$. $z/W = 0.5$. Lines: predictions; markers: experiments [1]

be compared to Aksevoll & Moin [19] and Yang & Ferziger [20] who used 50 and and 3.8 corresponding characteristic time units, respectively. It should be remembered that they, in addition, performed spanwise averaging, as their flows were homogeneous in the spanwise direction. The time T_{aver} in the present work is similar to that used in Ref. [20], but considerably shorter than that used in Ref. [19]. In those studied, however, they also present correlations of resolved fluctuations, which usually require considerably longer averaging times.

In Fig. 9 the time history of the reattachment point x_R at the center plane is shown. It can be seen that x_R fluctuates much. No information on the time history for this Re number is provided in Ref. [1]. Romano *et al.* [15] present time history of x_R in their configuration ($h/H = 2/3$ and $Re = 2500$), and they find that $x_R/(H-h)$ oscillates between 2 and 10. In the DNS simulations of Le *et al.* [21] ($h/H = 1/2$ and $Re = 5000$) they find that $x_R/(H-h)$ oscillates between 5 and 8.

In Figs. 10 and 11 the three-dimensionality of the flow field is illustrated. The contours of the $\langle\bar{u}\rangle_t$ velocity contours close to zero are shown near the ceiling and near the floor (Fig. 10). We find that the main reattachment line is fairly straight for both Re numbers. There is larger spanwise variation for the secondary recirculation bubble below the inlet. The separation line for this bubble is $x_R/H \simeq 3$ and 2 for $Re = 780$ and $Re = 5000$, respectively. For the high Reynolds number there is no separation along the ceiling. However, for $Re = 780$ we find separation along the side walls up to $0.8H$ from the walls, see Fig. 10a. In the center plane, however, no separation takes place, which can also be seen from the vector field in Fig. 3. Note that we are here taking about *time averaged* flow field. *Instantaneously* there are negative $\bar{u}$ velocities near the ceiling. The instantaneous recirculating regions are very thin, however.

In Fig. 11 time averaged $\bar{u}$ profiles along spanwise lines are shown. It can be seen that the flow is not two-dimensional, but there are spanwise variations of up to approximately 10% of the inlet velocity.

Fig. 12 show the time-averaged skin friction along the centerline. This is similar to the skin friction presented in Ref. [21].

6 Conclusions

Large Eddy Simulations of the backwards-facing flow with a large step $h/H = 1/6$, have been presented for two different Reynolds number $Re = 780$ and $Re = 5000$.

Unfortunately, we believe that the experiments at this low-Re number should be regarded with some caution, because it has been found that the corresponding experimental investigation for laminar condition ($Re = 117$) are likely to be incorrect [5].

For $Re = 780$ the predictions show that the flow close to the inlet is close to laminar ($u_{rms} \simeq 0.01$), and that further downstream the flow becomes fully turbulent ($u_{rms} \simeq 0.11$). The predicted recirculation region is larger than for $Re = 5000$, an observation which has some support in the literature [14][15].

It has previously been found that the $k-\varepsilon$ model cannot handle this type of flow, and no convergent solutions are obtained [16]. The reason is that the ε does not have any solution when $k \to 0$, because it includes terms like ε/k. On the other hand, the $k-\omega$ model has been shown to perform better, and

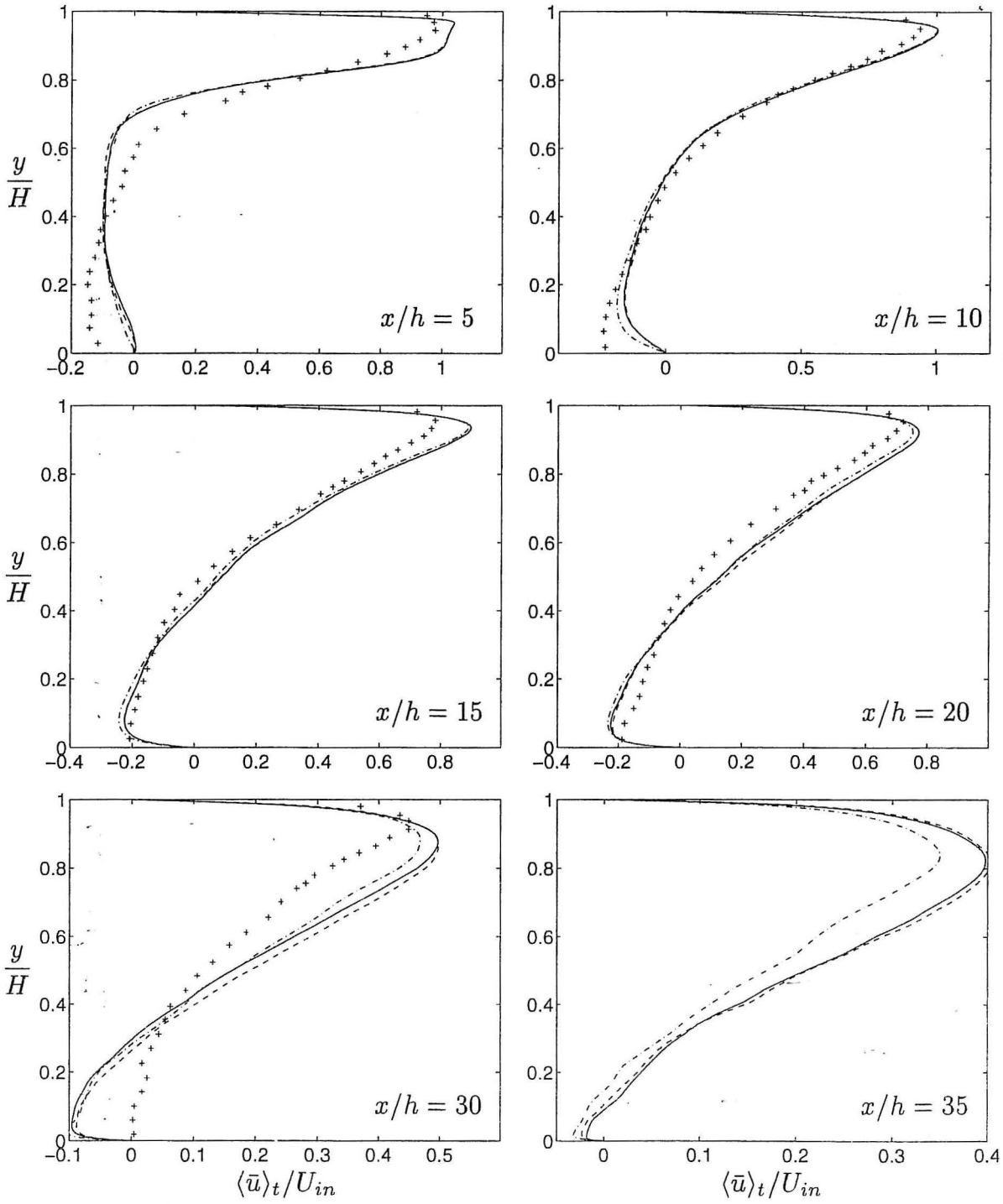

Figure 5: Time averaged streamwise velocity $\langle \bar{u} \rangle_t$. $Re = 5000$. $z/W = 0.5$. Solid lines: time averaged during 17 000 time steps ($128 \times 80 \times 80$); dashed lines: time averaged during 11 000 time steps ($128 \times 80 \times 80$); dash-dotted lines: time averaged during 18 000 time steps ($128 \times 80 \times 128$); markers: experiments [1]

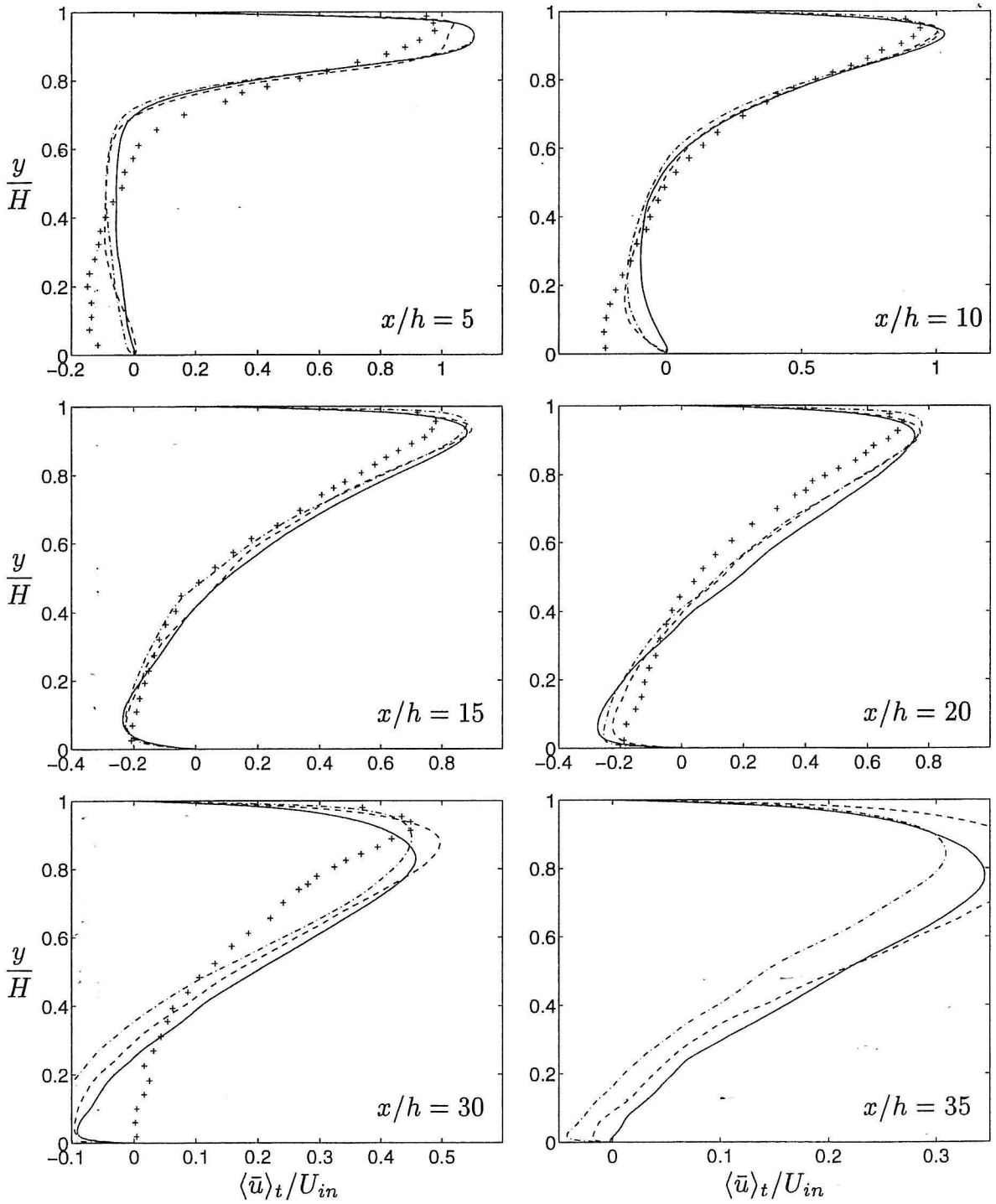

Figure 6: Time averaged streamwise velocity $\langle \bar{u} \rangle_t$. $Re = 5000$. $z/W = 0.5$. Solid lines: constant inlet profile (Eq. 9), dynamic one-equation model; dashed lines: 1/7 profile, dynamic one-equation model; dash-dotted lines: 1/7 profile, dynamic model [6]; markers: experiments [1]

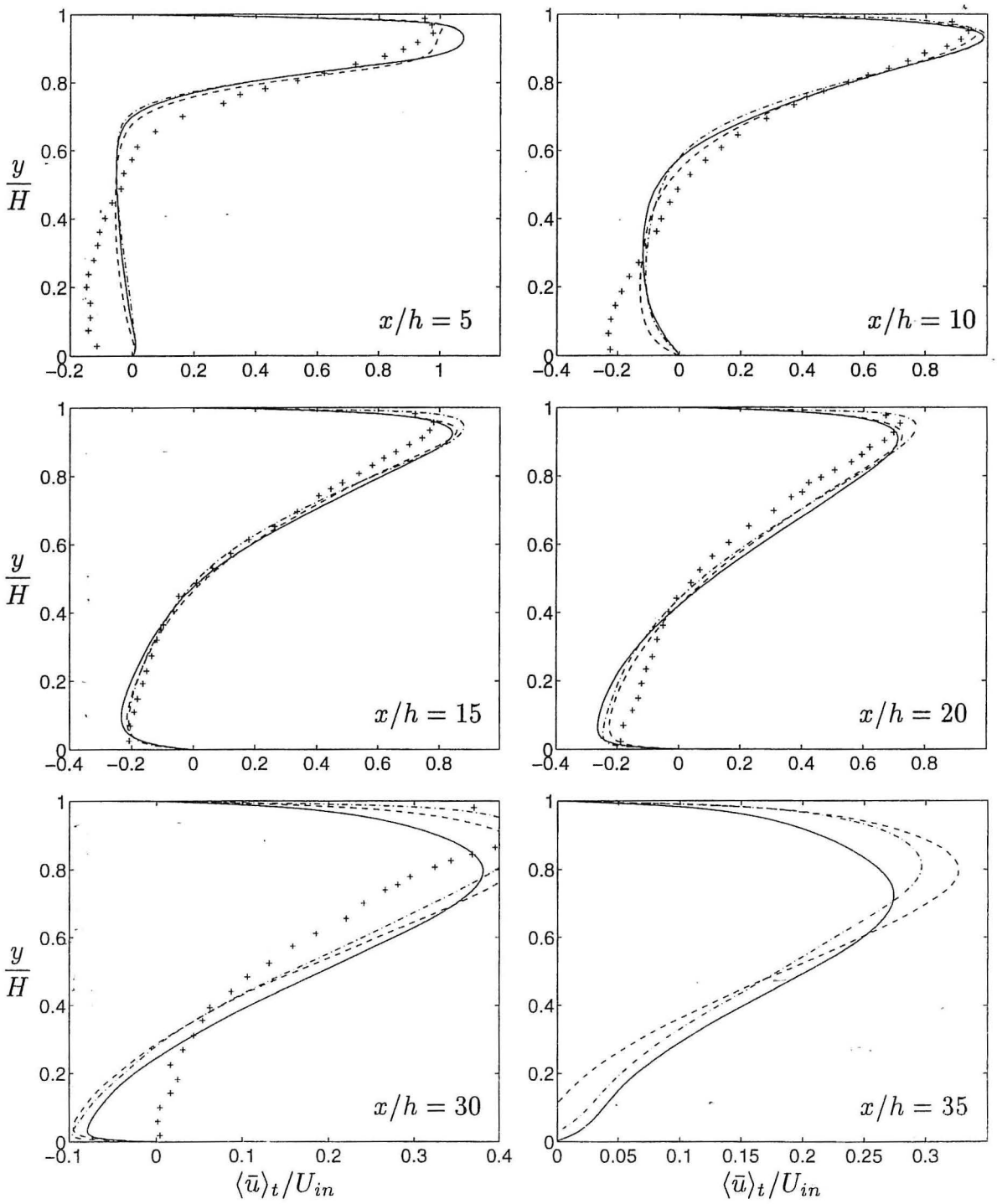

Figure 7: Time averaged streamwise velocity $\langle \bar{u} \rangle_t$. Spanwise averaged over $2H$. $Re = 5000$. Solid lines: constant inlet profile (Eq. 9), dynamic one-equation model; dashed lines: 1/7 profile, dynamic one-equation model; dash-dotted lines: 1/7 profile, dynamic model [6]; markers: experiments [1]

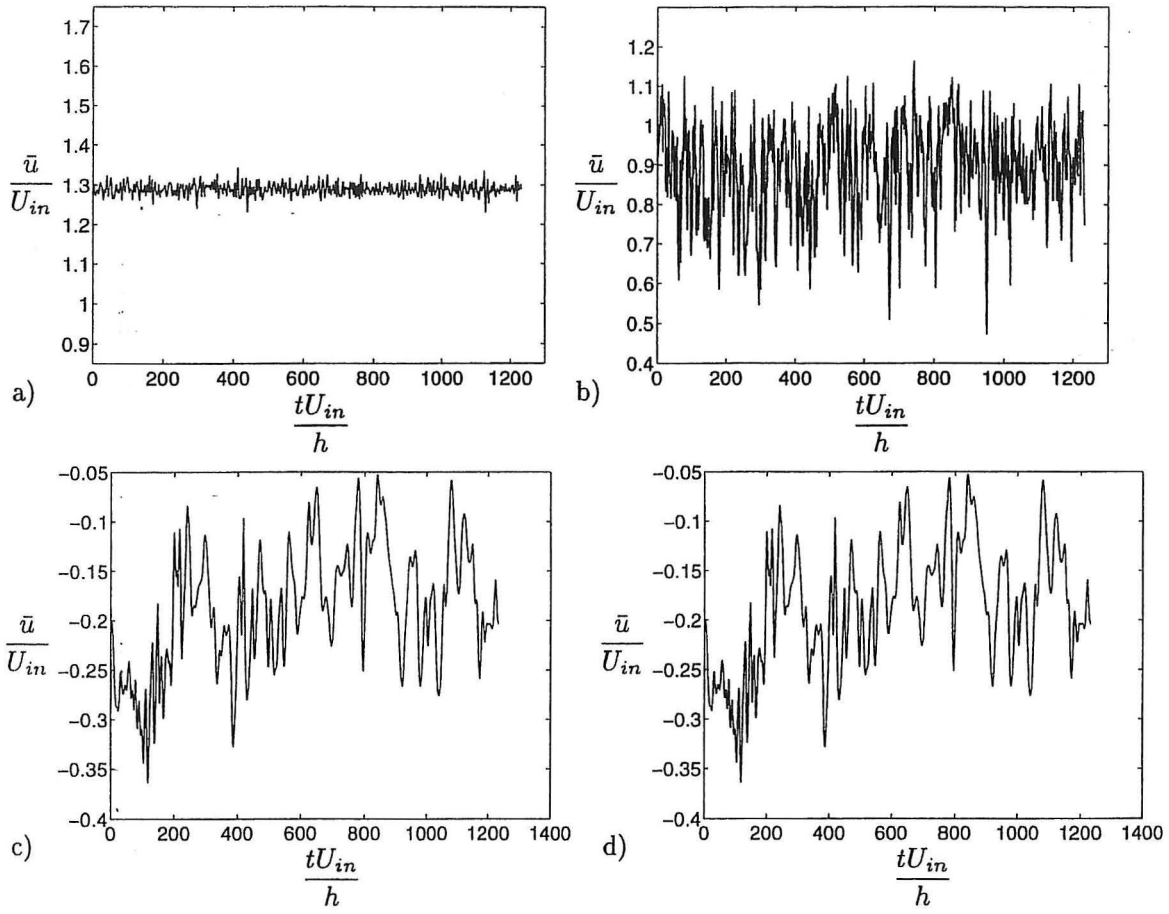

Figure 8: Time history of the $\bar{u}$ velocity at two chosen points. $z/W = 0.5$. $Re = 780$. a) $x/H = 5/6$, $y = 0.92H$. b) $x/H = 4$, $y = 0.92H$. c) $x/H = 5/6$, $y = 0.14$. d) $x/H = 4$, $y = 0.14$.

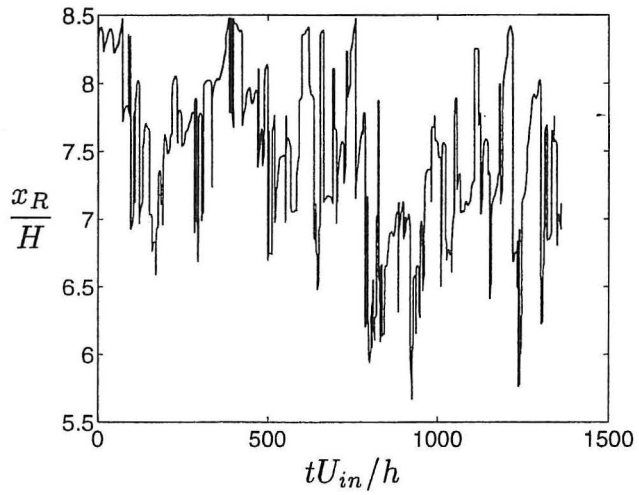

Figure 9: Time history of position of reattachment x_R. $Re = 5000$. $z/W = 0.5$.

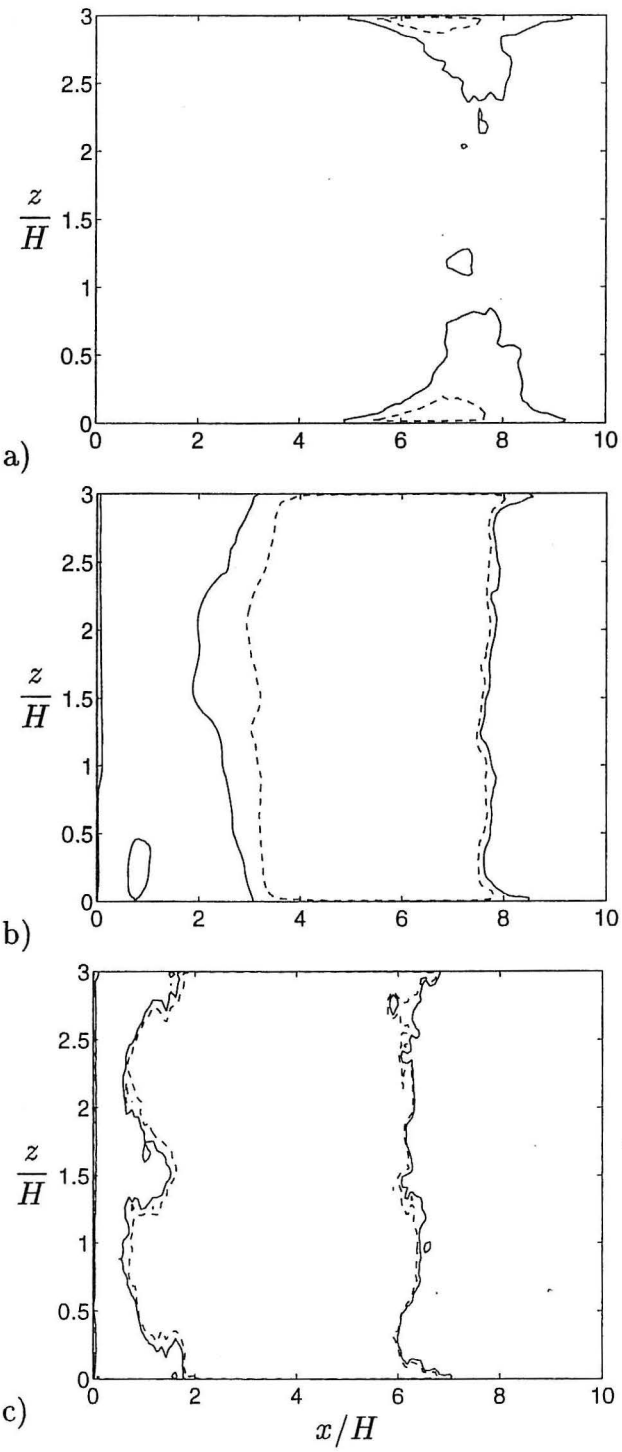

Figure 10: Contours of time averaged streamwise velocity $\langle \bar{u} \rangle_t$ at the near-wall node. Solid line: $\langle \bar{u} \rangle_t = 0$; dashed line: $\langle \bar{u} \rangle_t / U_{in} = -0.002$. a) Ceiling, $Re = 780$. b) Floor, $Re = 780$. c) Floor, $Re = 5000$.

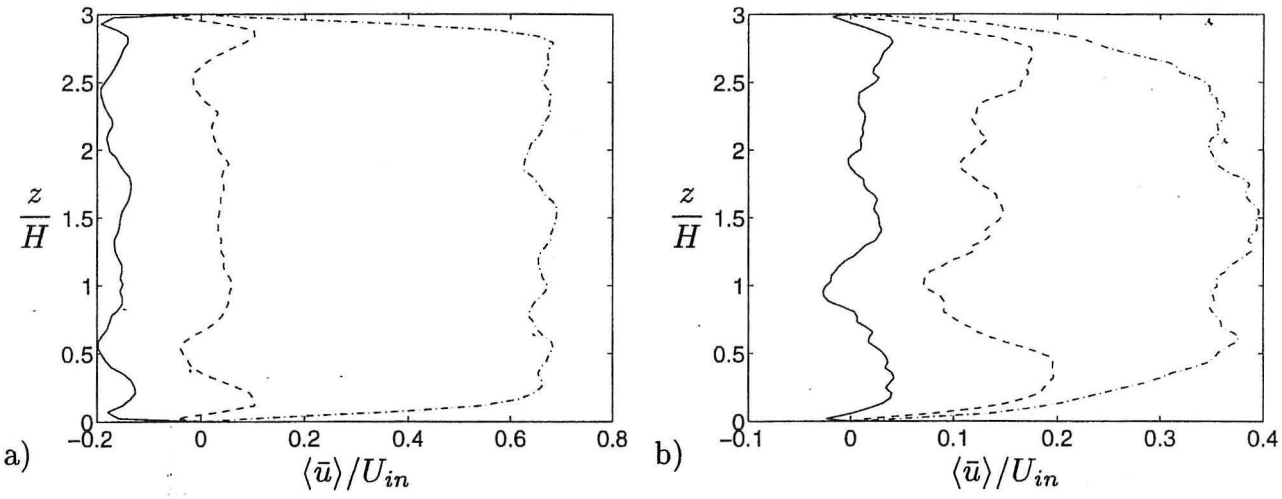

Figure 11: Time-averaged $\bar{u}$ velocity. $x/H = 6$. Solid line: $y/H = 0.16$; dashed line: $y/H = 0.4$; dash-dotted line: $y/H = 0.85$. a) $Re = 780$. b) $Re = 5000$.

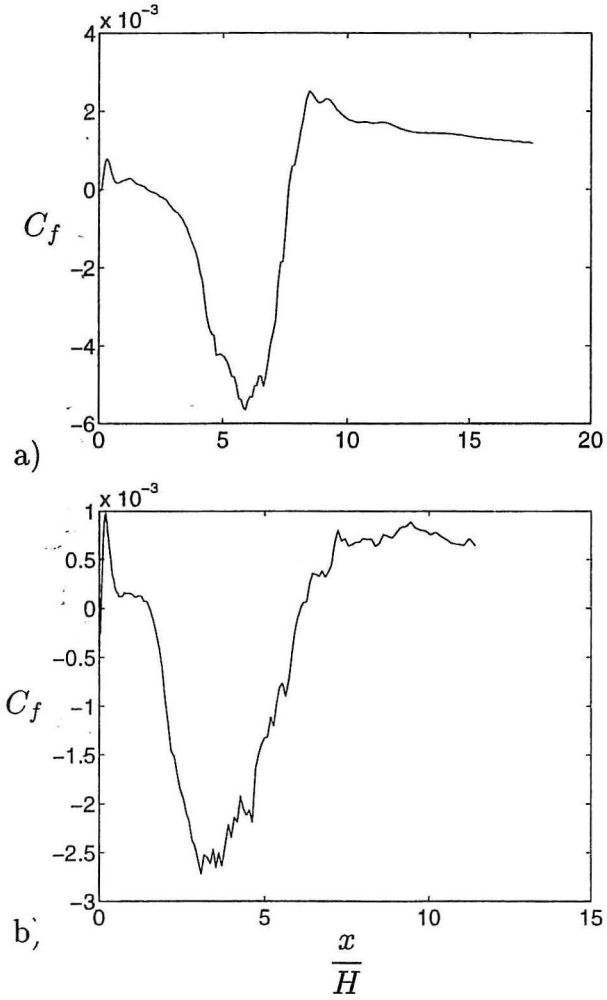

Figure 12: Time-averaged skin friction along the floor. $z/W = 0.5$. a) $Re = 780$. b) $Re = 5000$.

convergent solutions were obtained [18]. The $k-\omega$ model gave [18], as in the present work, an increasing x_R with decreasing Re.

At the high Reynolds number $Re = 5000$ the agreement between predictions and experiments are fairly good, except in the reattachment region. The predicted recirculation region is some 20% larger than the experimental one. The reason for this discrepancy is not clear.

References

[1] A. Restivo. *Turbulent Flow in Ventilated Rooms.* PhD thesis, University of London, Imperial College of Science and Technology, Mechanical Engineering Department, 1979.

[2] L. Davidson and P. Nielsen. Large eddy simulations of the flow in a three-dimensional ventilated room. In S. Murakami, editor, *5th Int. Conf. on Air Distributions in Rooms, ROOMVENT'96*, volume 2, pages 161–168, Yokohama, Japan, 1996.[1]

[3] L. Davidson. LES of recirculating flow without any homogeneous direction: A dynamic one-equation subgrid model. In K. Hanjalić and T.W.J. Peeters, editors, *2nd Int. Symp. on Turbulence Heat and Mass Transfer*, pages 481–490, Delft, 1997. Delft University Press.[1]

[4] L. Davidson. Large eddy simulation: A dynamic one-equation subgrid model for three-dimensional recirculating flow. In *11th Int. Symp. on Turbulent Shear Flow*, volume 3, pages 26.1–26.6, Grenoble, 1997.[1]

[5] L. Davidson and P.V. Nielsen. A study of laminar backward-facing step flow. Report, Dept. of Building Technology and Structural Engineering, Aalborg University, 1998.[1]

[6] M. Germano, U. Piomelli, P. Moin, and W.H. Cabot. A dynamic subgrid-scale eddy viscosity model. *Physics of Fluids A*, 3:1760–1765, 1991.

[7] M. Germano, U. Piomelli, P. Moin, and W.H. Cabot. Erratum. *Physics of Fluids A*, 3:3128, 1991.

[8] S. Ghosal, T.S. Lund, P. Moin, and K. Akselvoll. A dynamic localization model for large-eddy simulation of turbulent flows. *Journal of Fluid Mechanics*, 286:229–255, 1995.

[9] S. Ghosal, T.S. Lund, P. Moin, and K. Akselvoll. Corrigendum. *Journal of Fluid Mechanics*, 297:402, 1995.

[10] L. Davidson. Large eddy simulations: A note on derivation of the equations for the subgrid turbulent kinetic energies. Rept. 97/11, Dept. of Thermo and Fluid Dynamics, Chalmers University of Technology, Gothenburg, 1997.[1]

[11] L. Davidson and B. Farhanieh. CALC-BFC: A finite-volume code employing collocated variable arrangement and cartesian velocity components for computation of fluid flow and heat transfer in complex three-dimensional geometries. Rept. 92/4, Dept. of Thermo and Fluid Dynamics, Chalmers University of Technology, Gothenburg, 1992.[1]

[12] A. Sohankar, C. Norberg, and L. Davidson. Low-Reynolds number flow around a square cylinder at incidence: Study of blockage, onset of vortex shedding and outlet boundary condition. *International Journal for Numerical Methods in Fluids*, 26:39–56, 1998.

[13] I. Zacharov. private communication. European Supercomputer Team, Silicon Graphics Inc., Switzerland, 1997.

[14] B.F. Armaly, F. Durst, J.C.F. Pereira, and B. Schönung. Experimental and theoretical investigation of backward-facing step flow. *Journal of Fluid Mechanics*, 127:473–496, 1983.

[15] G.P. Romano, S. Pomponio, and G. Querzoli. An investigation on the fluctuations of the reattachment point downstream backward facing step using particle tracking velocimetry. In *11th Int. Symp. on Turbulent Shear Flow*, volume 3, pages 30.7–30.12, Grenoble, 1997.

[16] M. Skovgaard and P.V. Nielsen. Numerical investigation of transitional flow over a backward facing step using a low Reynolds number $k - \varepsilon$ model. In *12th AIVC-Conference on Air Movement Control within Buildings*, Ottawa, Canada, 1991.

[17] S-H Peng, L. Davidson, and S. Holmberg. A modified Low-Reynolds-Number $k - \omega$ model for recirculating flows. *ASME: Journal of Fluids Engineering*, 119:867–875, 1997.

[18] S.-H. Peng, L. Davidson, and S. Holmberg. The two-equations turbulence $k-\omega$ model applied to recirculating ventilation flows. Rept. 96/13, Dept. of Thermo and Fluid Dynamics, Chalmers University of Technology, Gothenburg, 1996.[1]

[19] K. Akselvoll and P. Moin. Large eddy simulation of turbulent confined coannular jets and turbulent flow over a backward facing step. Report no. TF-63, Stanford University, Dept. Mech. Eng., 1995.

[20] K.-S. Yang and J.H. Ferziger. Large-eddy simulation of turbulent obstacle flow using a dynamic subgrid-scale model. *AIAA Journal*, 31:1406–1413, 1993.

[21] H. Le, P. Moin, and J. Kim. Direct numerical simulation of turbulent flow over a backward-facing step. *Journal of Fluid Mechanics*, 330:349–374, 1997.

[1] postscript file at http://www.tfd.chalmers.se/~lada

ISSN 1395-7953 R9842
Dept. of Building Technology and Structural Engineering
Aalborg University, October 1998
Sohngaardsholmsvej 57, DK-9000 Aalborg, Denmark
Phone: +45 9635 8080 Fax: +45 9814 8243
http://iee.civil.auc.dk